ARTICLE

Resonant Coherent Phonon Generation in Single-Walled Carbon Nanotubes through Near-Band-Edge Excitation

Yong-Sik Lim,[†,*] Jae-Geum Ahn,[†] Ji-Hee Kim,[‡] Ki-Ju Yee,[‡] Taiha Joo,[§] Sung-Hoon Baik,[⊥] Erik H. Hároz,[∥] Layla G. Booshehri,[∥] and Junichiro Kono[∥,*]

[†]Department of Applied Physics, Konkuk University, Chungju, Chungbuk 380-701, Republic of Korea, [‡]Department of Physics, Chungnam National University, Daejeon 305-764, Republic of Korea, [§]Department of Chemistry, POSTECH, Pohang 790-784, Republic of Korea, [⊥]Quantum Optics Research Division, Korea Atomic Energy Research Institute, Daejeon 305-353, Republic of Korea, and [∥]Department of Electrical and Computer Engineering, Rice University, Houston, Texas 77005

ABSTRACT We have observed large-amplitude coherent phonon oscillations of radial breathing modes (RBMs) in single-walled carbon nanotubes excited through the lowest-energy (E_{11}) interband transitions. In contrast to the previously studied coherent phonons excited through higher-energy (E_{22}) transitions, these RBMs show comparable intensities between $(n-m)$ mod 3 = +1 and −1 nanotubes. We also find the novel observation of RBMs excited over an excitation range of ~300 meV above the E_{11} transition, which we attribute to possible resonance with phonon sidebands of the lowest optical transition, arising from strong exciton−phonon coupling.

KEYWORDS: single-walled carbon nanotubes · coherent phonons · pump−probe spectroscopy · phonon sidebands · photoluminescence

Single-walled carbon nanotubes (SWNTs) are one of the most ideal one-dimensional systems available today for studying the effects of quantum confinement on carriers and phonons and their mutual interactions.[1,2] Advances in optical studies such as photoluminescence excitation (PLE) spectroscopy and resonant Raman scattering have led to definitive assignments of spectral features to specific chiralities, or (n,m).[3−6] Recent theoretical and experimental studies illuminate the importance of pronounced excitonic effects in interband optical processes in SWNTs due to their one-dimensionality as evidenced by observations of large exciton binding energies and nonemissive or "dark" exciton states.[6−10] Furthermore, PLE microscopy, polarized PLE, and photoconductivity studies have revealed a variety of phonon-assisted peaks,[11−13] suggesting strong exciton−phonon coupling.

Recently, we reported the observation of coherent phonon (CP) oscillations of radial breathing modes (RBMs) in SWNTs generated *via* impulsive excitation of E_{22} optical transitions.[14−16] We found that $(n-m)$ mod 3 ≡ ν = −1 tubes have much larger intensities than ν = +1 tubes, the same trend as seen in resonant Raman spectroscopy studies.[17−19] We also showed that CP spectroscopy has several advantages over Raman spectroscopy, including no Rayleigh scattering and PL backgrounds. Here, we use these advantages to study CP oscillations of RBMs in smaller-diameter SWNTs, synthesized by the CoMoCAT method, which showed E_{11} transitions within the wavelength range accessible with a Ti:sapphire laser. The data displayed several RBMs resonantly excited by the E_{11} and E_{22} transitions, as well as RBMs excited over widespread intermediate energies between the E_{11} and E_{22} optical transitions that may be due to phonon sidebands of the E_{11} transition.

RESULTS AND DISCUSSION

Figure 1a,b shows CP oscillations of RBMs resonantly excited through E_{11} and E_{22} optical transitions at selected excitation wavelengths within the 720−1000 nm range. Each trace shows a strong beating pattern due to the simultaneous excitation of multiple RBMs, which sensitively changes with the photon energy, implying that the CP oscillations are dominated by a few resonantly excited RBMs. It should be noted that, at long wavelengths (Figure 1b), the data show a normalized differential transmission ($\Delta T/T$) of the order of ~10^{-4} near time zero, which is 2−3 times larger than that for shorter wavelength excitation (Figure 1a).

Figure 2a shows contour plots of the CP intensity on a log scale as a function of photon energy [1.23 eV (1000 nm)−1.71 eV (720 nm)] and RBM frequency (155−400 cm^{-1}), obtained through a Linear Predic-

*Address correspondence to kono@rice.edu, yslim@kku.ac.kr.

Received for review January 10, 2010 and accepted April 27, 2010.

Published online May 14, 2010. 10.1021/nn100055e

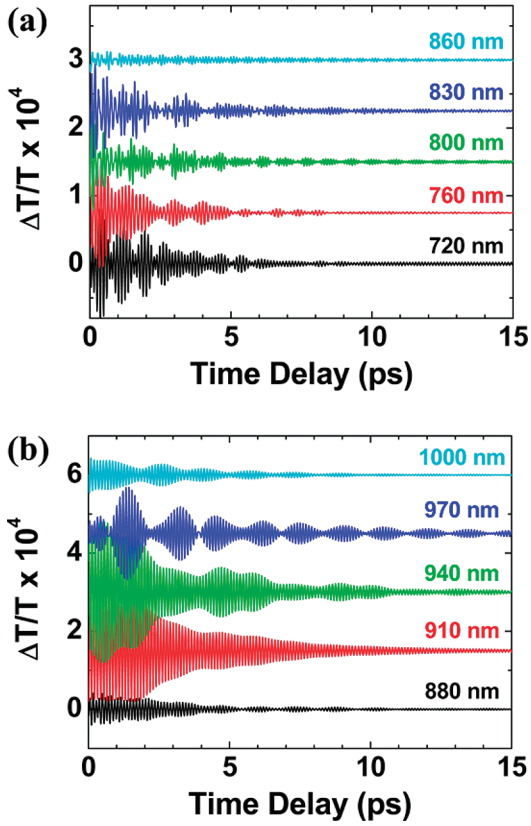

Figure 1. Coherent phonon oscillations measured at center wavelengths of (a) 720, 760, 800, 830, and 860 nm and (b) 880, 910, 940, 970, and 1000 nm, using degenerate pump and probe pulses.

tive Singular Value Decomposition (LPSVD) analysis on the measured time-domain data (see Supporting Information for more details). Here, rectangular symbols represent E_{22} transitions, and triangular symbols represent E_{11} transitions.[3] Red and white symbols are for $\nu = -1$ tubes, while blue and black symbols are for $\nu = 1$ tubes. Figure 2b,c shows representative CP spectra corresponding to horizontal cuts of the contour map in Figure 2a. Figure 2b shows CP spectra for excitation wavelengths of 720−740 nm with a step size of 5 nm, exhibiting three dominant RBMs between 240 and 280 cm^{-1}, all of which are E_{22}-excited, $\nu = -1$ tubes. Specifically, they belong to the $(2n + m) = 22$ family, that is, (11,0)/(10,2), (9,4), and (8,6) tubes having frequencies of 267/266.1, 258.3, and 246.6 cm^{-1}, respectively. The peak at 306 cm^{-1} is primarily due to the E_{22}-excited RBM of (9,1) tubes ($E_{22} \sim 1.76$ eV), with some contribution from (6,5) tubes excited between E_{11} and E_{22} (as described later). The black curve in Figure 2c was taken with 765 nm (1.62 eV) excitation, showing E_{22}-excited CPs for the $(2n + m) = 25$ family [(12,1), (11,3), and (10,5)] with frequencies between 220 and 240 cm^{-1}, as well as for the $(2n + m) = 28$ family [(14,0)/(13,2) and (12,4)] at frequencies between 200 and 220 cm^{-1}. The red trace in Figure 2c is a CP spectrum measured at an excitation wavelength of 965 nm (1.28 eV), which shows two sharp RBMs at 307.5 and 329.7 cm^{-1} corresponding to the $\nu = +1$ chiralities (6,5) and (7,3), respectively. These modes are excited through the E_{11} optical transition and exhibit CP intensities surpassing that of similar diameter $\nu = -1$ chiralities such as (8,3).

To deduce quantitative information on how the CP signal changes with ν, chiral angle, diameter, and optical transitions (E_{22} *vs* E_{11}), we fully analyzed the resonance excitation profiles of the observed features in Figure 2a, taking into account the double-peak line shape arising from the first derivative of a Lorentzian (see ref 14 as well as Supporting Information for more details). Table 1 summarizes the results obtained from such analysis, showing the CP intensity, the resonance energy, the FWHM, the chirality, and the ν of each RBM feature. There are several distinguishing characteristics and trends in Table 1 that are worth discussing. First, we find contrasting results between E_{22}-excited and E_{11}-excited CPs: for E_{22}-excited CPs (*i.e.*, those excited at photon energies higher than 1.45 eV), $\nu = -1$ nano-

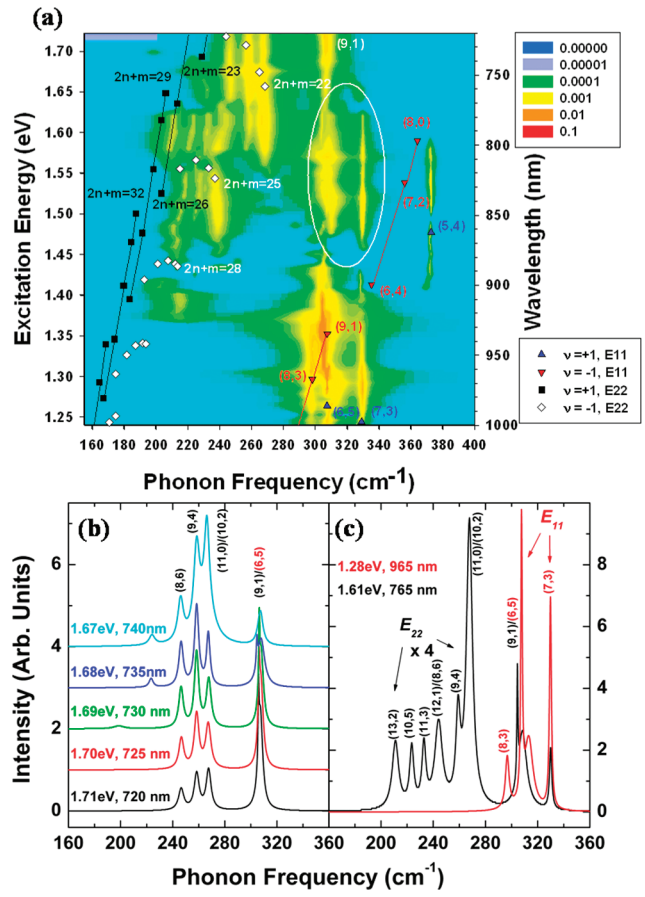

Figure 2. (a) Two-dimensional log plot of a Fourier transform of CP oscillations, retrieved through the LPSVD method, measured over a photon energy range of 720−1000 nm (1.71−1.23 eV) with a 5 nm step size. The rectangular symbols are for E_{22} transitions, and triangular symbols are for E_{11} transitions from ref 3. Both white and black symbols are for $\nu = +1$, while red and blue are for $\nu = -1$. (b) CP spectra measured at center wavelengths of 720, 725, 730, 735, and 740 nm, showing RBMs resonantly excited through E_{22} optical transitions. (c) Comparison of RBMs resonantly excited through E_{22} and E_{11} optical transitions with degenerate pump−probe pulses with center wavelengths at 765 and 965 nm, respectively.

TABLE 1. Summary of Observed Coherent Phonons of the Radial Breathing Mode

$(n,m)^a$	$2n+m^b$	ν^c	E_{ii}^d	ω_{RBM} $(cm^{-1})^e$	Γ $(meV)^f$	E_0 $(eV)^g$	I_0 $(au)^h$
(11,0)	22	−1	E_{22}	267	81.7	1.714	3.27
(10,2)	22	−1	E_{22}	266.1	77.5	1.713	2.83
(9,4)	22	−1	E_{22}	258.3	66.7	1.728	2.34
(8,6)	22	−1	E_{22}	246.6	73.6	1.732	1.35
(12,1)	25	−1	E_{22}	238.5	50.2	1.555	0.95
(11,3)	25	−1	E_{22}	231.9	51.2	1.565	0.43
(10,5)	25	−1	E_{22}	227.1	42.1	1.564	0.32
(14,0)	28	−1	E_{22}	215.1	63.9	1.434	0.33
(13,2)	28	−1	E_{22}	210.9	54.5	1.432	0.24
(12,4)	28	−1	E_{22}	208.8	54.0	1.432	0.16
(9,1)	19	−1	E_{11}	304.5	27.2	1.352	5.28
(8,3)	19	−1	E_{11}	297.6	52.4	1.286	2.55
(7,3)	17	+1	E_{11}	329.7	54.2	1.248	4.34
(6,5)	17	+1	E_{11}	307.5	27.4	1.281	3.37
(5,4)	14	+1	E_{11}	372.9	34.3	1.49	0.64

[a]Chirality indices. [b]Chirality family. [c]$\nu = (n - m)$ mod 3: chirality type. [d]Transition type. [e]Phonon frequency. [f]Full width at half maximum (fwhm) of excitation profile. [g]Transition energy. [h]Calculated Lorentzian strength.

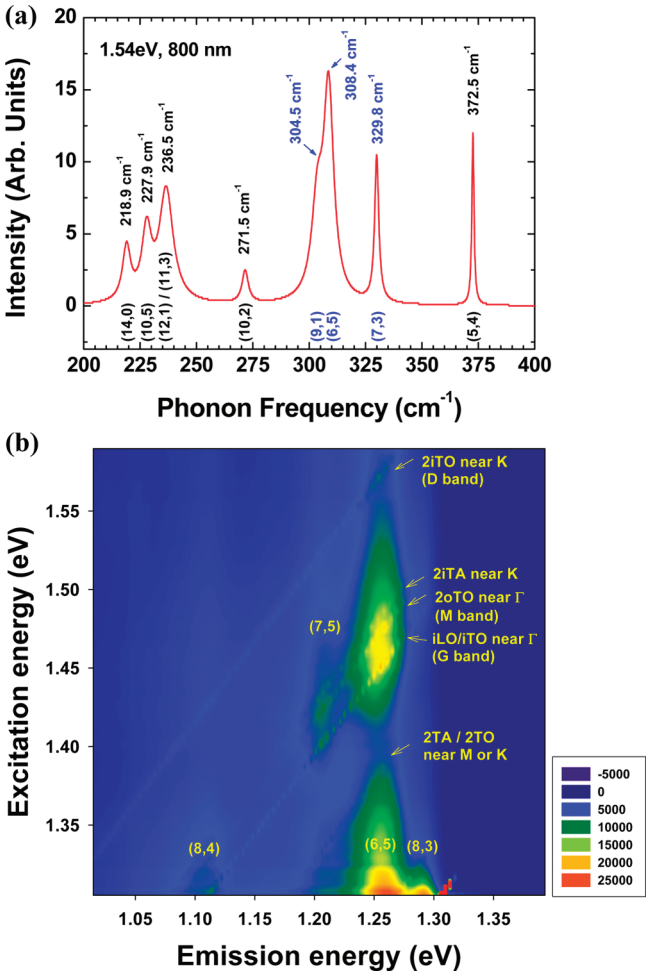

Figure 3. (a) CP spectrum measured with a center wavelength of 800 nm (1.54 eV). Strong, phonon-sideband-excited RBMs are indicated by blue lettering. (b) PLE spectra for (6,5) tubes in the same CoMoCAT sample as used in the CP experiments. The dotted linear lines indicate emissions *via* resonant Raman processes with multiple phonon bands such as G-band, M-band, and D-band.

tubes show markedly higher intensities than $\nu = +1$ nanotubes (the latter are nearly invisible in the spectra), whereas for E_{11}-excited CPs (*i.e.*, those excited at photon energies lower than 1.45 eV), the intensities are comparable between the $\nu = -1$ and $\nu = +1$ nanotubes. The E_{11}-excited RBMs for $\nu = +1$ near-armchair tubes such as (6,5) or (5,4) are very strong. It is interesting that the RBM peak due to (7,3) tube with $\nu = +1$ is 2 times stronger than the (8,3) tube with $\nu = -1$ even though they possess similar diameters and chiral angles. Second, we note that, for E_{22}-excited tubes, the CP intensity varies strongly within each family as a function of chiral angle. Namely, the intensity tends to decrease as the chiral angle increases (going from zigzag to armchair). This trend is the same as we observed earlier for HiPco samples[14] and can be explained through the chiral-angle dependence of the exciton−phonon coupling matrix.[7,20,21] Third, we see the intensity decrease of E_{22}-excited CPs as the $(2n + m)$ family index increases from 22 (~0.9 nm in diameter) to 28 (~1.1 nm in diameter), which is opposite to what was observed for HiPco nanotubes.[14] We note that the different diameter distributions, which depend on the particular growth conditions of each material, may be the reason for the different strength trends between HiPco and CoMoCAT nanotubes with mean diameter of 1.0 and 0.8 nm, respectively. Fourth, the intensity of E_{11}-excited RBMs appears to have the same type of chiral-angle dependence as E_{22}-excited RBMs within the same family. This can be most clearly seen by comparing (6,5) and (7,3) tubes (both are family 17 tubes). Although (6,5) is the most populous species in our ensemble sample, its intensity is smaller than that for (7,3) tubes. Fifth, $\nu = -1$ nanotubes such as (9,1) show CP intensities that are comparable irrespective of whether they are excited *via* the E_{11} or E_{22} optical transitions. These results are partially consistent with the previous theoretical predictions[7,20,21] and close to our recent microscopic CP theory,[16] but they serve to invite more accurate theoretical calculations.

Finally, we discuss our surprising observation of intense RBMs of the (6,5) and (7,3) chiralities, excited far away from their expected optical transitions over a wide energy range between the E_{11} and E_{22} transitions, indicated by the white ellipse in Figure 2a. Figure 3a shows CPs excited at 800 nm (1.54 eV). Compared with our previous CP study on HiPco samples, we observe several RBMs from CoMoCAT samples at frequencies higher than 280 cm^{-1}. We can readily assign the mode at 373 cm^{-1} to the RBM of the (5,4) tube with a diameter of 0.62 nm excited through the E_{11} optical transition. In addition, we observe excited RBMs at 304, 307, and 330 cm^{-1}, corresponding to (9,1), (6,5), and (7,3) tubes, respectively. Furthermore, these (6,5) and (7,3) spectral features are comparable in intensity to the same RBMs resonantly excited *via* E_{11} yet occur at energies more than 300 meV above their lowest optical transition.

These "off"-resonance-excited RBMs are also observed weakly for the (8,3) tube and likely to exist on the higher energy side of the E_{22} optical transition for some of the tubes of the $(2n + m) = 22$ and $(2n + m) = 25$ families, as shown in Figure 2a.

To investigate this spectral range more closely, we performed a PLE study on our sample over the excitation range of 775−945 nm (1.59−1.30 eV), as shown in Figure 3b. In the emission wavelength range of 885.5−1215.7 nm (1.39−1.01 eV), strong PL from the (6,5) tube, as well as weak PL from (7,5), (8,3), and (8,4) tubes, is observed. Our PLE spectra for the (6,5) tube do not show any notable PL signals at wavelengths (energies) near 952 nm (1.302 eV), 912 nm (1.359 eV), and 873 nm (1.42 eV), for which exciton energy transfer (EET) contributions may occur from the (8,3), (9,1), and/or (6,4) tubes, respectively.[22] Thus, we have excluded possible EET contributions from other tubes in our PLE analysis. On the basis of the dispersion curve of graphene,[23] we find additional PL contributions associated with two-phonon processes involving TA/TO phonons near the K or M edge at excitation as low as 1.39 eV (most likely from 2 oTA near the M edge). All phonon sidebands form straight dotted lines in the PLE contour map denoting emission from resonant Raman scattering processes. It should be noted in Figures 3b and 2a that the peak position of the dominant PLE signal for the (6,5) tube near 1.45 eV coincides with the discontinuous position in a resonance excitation profile (vertical line) of RBMs for (9,1)/(6,5) tubes, which also holds true for the (7,3) tube. Therefore, we believe this suggests that the strong RBM CP signals between the E_{11} and E_{22} transitions may be attributed to phonon sidebands due to several phonon-assisted emission processes above the E_{11} transition, which explains the observation of off-resonant RBMs appearing over almost the entire excitation range between the E_{11} and E_{22} transitions. The particular phonons that may be contributing to these CP signals is the subject of future work.

CONCLUSION

In conclusion, we have studied coherent phonon oscillations of radial breathing modes in micelle-suspended CoMoCAT single-walled carbon nanotubes with small diameters in the near-infrared from 1.23 to 1.71 eV. Unlike HiPco SWNTs, CoMoCAT SWNTs showed strong RBM CPs of semiconducting tubes resonantly excited through both E_{11} and E_{22} transitions within our excitation range. For excitation energies higher than 1.45 eV, semiconducting tubes of $\nu = -1$ dominantly showed resonant RBMs excited through the E_{22} transition, showing similar results to our previous study on HiPco samples. For excitation energies lower than 1.45 eV, we observed several RBMs of semiconducting tubes of both $\nu = -1$ and $\nu = +1$ types. We calculated relative spectral intensities by analyzing the resonance excitation profiles to demonstrate that the CP intensity shows the same chiral-angle dependence in both types. We also found that the CP intensity of $\nu = +1$ tubes varied strongly depending on whether it was excited through E_{11} or E_{22} transition, while $\nu = -1$ tubes did not show such variation. Finally, we observed strong, off-resonance-excited RBMs over a wide excitation range of more than 300 meV above the E_{11} transitions of (6,5) and (7,3) nanotubes, which we suggest as related to phonon sidebands due to multiple phonon-assisted excitonic transitions above the E_{11} transition observed through PLE measurements.

METHODS

Sample Preparation: The sample used in these studies was an aqueous suspension of CoMoCAT SWNTs prepared by a method similar to O'Connell *et al.*[24] Briefly, CoMoCAT SWNTs (SG65 grade, purchased from Southwest Nanotechnologies Inc.) were dispersed by ultrasonication (Cole-Parmer 500 W ultrasonic processor, model # CPX-600, 1/4 in. probe, 35% amplitude, 1 h) with a starting concentration of 0.2 mg/mL in 1% (wt/vol) sodium dodecylbenzene sulfonate (SDBS) in D_2O solvent. The SDBS micelle suspension was then ultracentrifuged for 2 h at 65 000*g* average (Sorvall Discovery 100SE ultracentrifuge using a Sorvall AH-629 swing bucket rotor). After ultracentrifugation, the upper 60% of the supernatant was removed and used for optical experiments. The absorption spectrum for our sample is shown in the Supporting Information and appears very similar to the data sheet presented on the manufacturer's Web site (http://www.swentnano.com/tech/docs/Final_SG_65_Data_Sheet.pdf) for SG65 material. On the basis of absorption, the sample nanotube concentration is estimated to be 15 mg/L. All optical measurements were performed on the above sample inside a quartz cuvette with a 1 mm path length.

Pump−Probe Spectroscopy Measurements: Multiple RBMs of SWNTs corresponding to different diameters were simultaneously excited within the broad 30−40 nm bandwidth of 40−50 fs pulses from a Ti:sapphire oscillator with a repetition rate of 90 MHz and an average power of 300−400 mW through degenerate pump−probe differential transmission spectroscopy. The pump and probe beams were kept at a total fixed power of 30 mW, divided by a beam splitter with a 7:3 ratio and were focused by a lens with a 5 cm focal length. A portion of the probe beam acted as the reference beam for one photodiode of a Nirvana balance detector, while the transmitted probe was aligned to the other photodiode. We tuned the center wavelength of the pump beam over a wide wavelength range of 720−1000 nm in steps of 5 nm to investigate the E_{11} and E_{22} transitions.[25] To get a high signal-to-noise ratio, we averaged multiple signals with a fast scanner of 20 Hz and a high speed data acquisition card. All signals were averaged over 10 000 scans at room temperature. A linear square fitting analysis method known as the linear prediction based on singular value decomposition (LPSVD),[26,27] which retrieves time constants shorter than the duration of the excitation pulse in the presence of noise, was applied for obtaining the resonance excitation profile to compare the magnitude of vibration strengths of resonantly excited RBMs between $\nu = +1$ and $\nu = -1$ semiconducting nanotubes (see Supporting Information for more details).

Photoluminescence Excitation Spectroscopy Measurements: Photoluminescence excitation spectroscopy was performed using excitation light in the wavelength range of 775−945 nm (1.59−1.30 eV), obtained from a cw Ti:sapphire laser (Mira 900-F, Coherent Inc.) with the fixed output power of 100 mW before the sample. Nanotube emission was measured from 885.5−1215.7 nm (1.39−1.01 eV) at each excitation through a spectrograph (SP-2500i, Acton Research) onto an InGaAs CCD array detector (1024-1.7, Princeton Instrument Inc.). Spectra were acquired with 5 and 2 nm steps in excitation and emission wavelengths, respectively. Individual spectra at each excitation wavelength were obtained over the entire emission range using a 30 s integration time. Spectra were corrected for power and instrument response.

Acknowledgment. This work was supported by the Korea Science and Engineering Foundation (KOSEF) grant funded by the Korean Government (MOST) (R01-2007-000-20651-0, 2008-03535, 2009-0085432), DOE-BES (through Grant No. DEFG02-06ER46308), the Robert A. Welch Foundation (Grant No. C-1509), and the National Science Foundation (OISE-0530220).

Supporting Information Available: Absorption spectrum of the sample used in this work as well more information on the linear prediction based on singular value decomposition (LPSVD) method that we used to retrieve time constants shorter than the duration of the excitation pulse and obtain resonance excitation profiles for coherent phonons. This material is available free of charge *via* the Internet at http://pubs.acs.org.

REFERENCES AND NOTES

1. Saito, R.; Dresselhaus, G.; Dresselhaus, M. S. *Physical Properties of Carbon Nanotubes*; Imperial College Press: London, 1998.
2. Reich, S.; Thomsen, C.; Maultzsch, J. *Carbon Nanotubes: Basic Concepts and Physical Properties*; Wiley-VCH: Berlin, 2004.
3. Bachilo, S. M.; Strano, M. S.; Kittrell, C.; Hauge, R. H.; Smalley, R. E.; Weisman, R. B. Structure-Assigned Optical Spectra of Single-Walled Carbon Nanotubes. *Science* **2002**, *298*, 2361–2366.
4. Fantini, C.; Jorio, A.; Souza, M.; Strano, M. S.; Dresselhaus, M. S.; Pimenta, M. A. Optical Transition Energies for Carbon Nanotubes from Resonant Raman Spectroscopy: Environment and Temperature Effects. *Phys. Rev. Lett.* **2004**, *93*, 147406.
5. Telg, H.; Maultzsch, J.; Reich, S.; Hennrich, F.; Thomsen, C. Chirality Distribution and Transition Energies of Carbon Nanotubes. *Phys. Rev. Lett.* **2004**, *93*, 177401.
6. Maultzsch, J.; Telg, H.; Reich, S.; Thomsen, C. Radial Breathing Mode of Single-Walled Carbon Nanotubes: Optical Transition Energies and Chiral-Index Assignment. *Phys. Rev. B* **2005**, *72*, 205438.
7. Reich, S.; Thomsen, C.; Robertson, J. Exciton Resonances Quench the Photoluminescence of Zigzag Carbon Nanotubes. *Phys. Rev. Lett.* **2005**, *95*, 077402.
8. Spataru, C. D.; Ismail-Beigi, S.; Benedict, L. X.; Louie, S. G. Excitonic Effects and Optical Spectra of Single-Walled Carbon Nanotubes. *Phys. Rev. Lett.* **2004**, *92*, 077402.
9. Wang, F.; Dukovic, G.; Brus, L. E.; Heinz, T. F. The Optical Resonances in Carbon Nanotubes Arise from Excitons. *Science* **2005**, *308*, 838–841.
10. Srivastava, A.; Htoon, H.; Klimov, V. I.; Kono, J. Direct Observation of Dark Excitons in Individual Carbon Nanotubes: Inhomogeneity in the Exchange Splitting. *Phys. Rev. Lett.* **2008**, *101*, 087402.
11. Kiowski, O.; Arnold, K.; Lebedkin, S.; Hennrich, F.; Kappes, M. M. Direct Observation of Deep Excitonic States in the Photoluminescence Spectra of Single-Walled Carbon Nanotubes. *Phys. Rev. Lett.* **2007**, *99*, 237402.
12. Lefebvre, J.; Finnie, P. Polarized Photoluminescence Excitation Spectroscopy of Single-Walled Carbon Nanotubes. *Phys. Rev. Lett.* **2007**, *98*, 167406.
13. Lebedkin, S.; Hennrich, F.; Kiowski, O.; Kappes, M. M. Photophysics of Carbon Nanotubes in Organic Polymer−Toluene Dispersions: Emission and Excitation Satellites and Relaxation Pathways. *Phys. Rev. B* **2008**, *77*, 165429.
14. Lim, Y.-S.; Yee, K.-J.; Kim, J.-H.; Haroz, E. H.; Shaver, J.; Kono, J.; Doorn, S. K.; Hauge, R. H.; Smalley, R. E. Coherent Lattice Vibrations in Single-Walled Carbon Nanotubes. *Nano Lett.* **2006**, *6*, 2696–2700.
15. Kim, J.-H.; Han, K.-J.; Kim, N.-J.; Yee, K.-J.; Lim, Y.-S.; Sanders, G. D.; Stanton, C. J.; Booshehri, L. G.; Haroz, E. H.; Kono, J. Chirality-Selective Excitation of Coherent Phonons in Carbon Nanotubes by Femtosecond Optical Pulses. *Phys. Rev. Lett.* **2009**, *102*, 037402.
16. Sanders, G. D.; Stanton, C. J.; Kim, J.-H.; Yee, K.-J.; Lim, Y.-S.; Haroz, E. H.; Booshehri, L. G.; Kono, J.; Saito, R. Resonant Coherent Phonon Spectroscopy of Single-Walled Carbon Nanotubes. *Phys. Rev. B* **2009**, *79*, 205434.
17. Goupalov, S. V.; Satishkumar, B. C.; Doorn, S. K. Excitation and Chirality Dependence of the Exciton−Phonon Coupling in Carbon Nanotubes. *Phys. Rev. B* **2006**, *73*, 115401.
18. Telg, H.; Maultzsch, J.; Reich, S.; Thomsen, C. Resonant Raman Intensities and Transition Energies of the E_{11} Transition in Carbon Nanotubes. *Phys. Rev. B* **2006**, *74*, 115415.
19. Satishkumar, B. C.; Goupalov, S. V.; Haroz, E. H.; Doorn, S. K. Transition Level Dependence of Raman Intensities in Carbon Nanotubes: Role of Exciton Decay. *Phys. Rev. B* **2006**, *74*, 155409.
20. Popov, V. N.; Henrard, L.; Lambin, P. Resonant Raman Intensity of the Radial Breathing Mode of Single-Walled Carbon Nanotubes within a Nonorthogonal Tight-Binding Model. *Nano Lett.* **2004**, *4*, 1795–1799.
21. Jiang, J; Saito, R; Gruneis, A; Chou, S. G; Samsonidze, Ge. G; Jorio, A; Dresselhaus, G; Dresselhaus, M. S. Intensity of the Resonance Raman Excitation Spectra of Single-Wall Carbon Nanotubes. *Phys. Rev. B* **2005**, *71*, 205420.
22. Tan, P. H.; Rozhin, A. G.; Hasan, T.; Hu, P.; Scardaci, V.; Milne, W. I.; Ferrari, A. C. Photoluminescence Spectroscopy of Carbon Nanotubes Bundles: Evidence for Exciton Energy Transfer. *Phys. Rev. Lett.* **2007**, *99*, 137402.
23. Chou, S. G. Phonon-Assisted Excitonic Recombination Channels Observed in DNA-Wrapped Carbon Nanotubes Using Photoluminescence Spectroscopy. *Phys. Rev. Lett.* **2005**, *94*, 127402.
24. O'Connell, M. J.; Bachilo, S. M.; Huffman, C. B.; Moore, V. M.; Strano, M. S.; Haroz, E. H.; Rialon, K. L.; Boul, P. J.; Noon, W. H.; Kittrell, C.; Ma, J.; Hauge, R. H.; Weisman, R. B.; Smalley, R. E. Band-Gap Fluorescence from Individual Single-Walled Carbon Nanotubes. *Science* **2002**, *297*, 593–596.
25. Ruppert, C.; Betz, M. Generation of 30 fs, 900−970 nm Pulses from a Ti:Sapphire Laser Far Off the Gain Peak. *Opt. Exp.* **2008**, *16*, 5572–5576.
26. Barkhuijsen, H.; De Beer, R.; Van Ormondt, D. Improved Algorithm for Noniterative Time-Domain Model Fitting to Exponentially Damped Magnetic Resonance Signals. *J. Magn. Reson.* **1987**, *73*, 553–557.
27. Wise, F. W.; Rosker, M. J.; Millhauser, G. L.; Tang, C. L. Application of Linear Prediction Least-Squares Fitting to Time-Resolved Optical Spectroscopy. *IEEE J. Quantum Electron.* **1987**, *23*, 1116–1121.